PHYSICAL REVIEW D VOLUME 18, NUMBER 11 1 DECEMBER 1978

Asymmetries in inclusive proton-nucleon scattering at 11.75 GeV/c

W. H. Dragoset, Jr. and J. B. Roberts
Department of Physics and T. W. Bonner Nuclear Laboratory, Rice University, Houston, Texas 77005

J. E. Bowers, H. W. Courant, H. Kagan, M. L. Marshak, E. A. Peterson, and K. Ruddick
School of Physics and Astronomy, University of Minnesota, Minneapolis, Minnesota 55455

R. D. Klem
Accelerator Research Facilities Division, Argonne National Laboratory, Argonne, Illinois 60439
(Received 21 November 1977)

We have measured the left-right asymmetry for the inclusive production of $\pi^{\pm}$, $K^{\pm}$, and protons in proton-proton and proton-deuteron collisions at 11.75 GeV/c. The measurements, utilizing the polarized proton beam at the Argonne zero-gradient synchrotron, cover a wide range of kinematic variables [u between 0.6 and -1.5 (GeV/c)^2 and x between 0.1 and 0.9 for meson production, t between -0.2 and -2.0 (GeV/c)^2 and x between -0.25 and 0.75 for proton production]. There is considerable angular structure in the pion-production data but not in the kaon or proton processes. Proton production alone is clearly sensitive to the isotopic spin of the target particle. A simple phenomenological model of baryon-exchange dominance successfully relates the inclusive pion asymmetries to the asymmetries in backward pion-nucleon elastic scattering. A triple-Regge model for the inclusive proton asymmetries is also discussed.

I. INTRODUCTION

In a high-energy proton-proton collision, most final states available to the reaction involve a large number of particles. In order to simplify the discussion of these reactions, an inclusive cross section can be defined in which attention is focused upon one type of particle produced in a particular state. Although these studies have been carried out for some years,[1] they have become increasingly important as the bombarding energies have risen through the construction of new accelerators. These experiments have provided support for parton models of elementary particles, for the existence of a hadronic temperature, and for the extension of Regge-exchange models to the triple-Regge picture.

These successes have naturally raised the question of whether the models can be extended to predict the left-right asymmetry observed when either the projectile or target proton is polarized. An early inclusive experiment, which used a polarized target,[2] did not allow a definitive test due to the large systematic errors which result from subtracting the effects of the nonhydrogenous material in the target. The advent of the polarized proton beam at the Argonne Zero Gradient Synchrotron (ZGS), however, has permitted several accurate inclusive experiments. In particular, the triple-Regge or Mueller-Regge model for proton production which is valid in the limit $s \to \infty$, m_X^2 large and $m_X^2/s \ll 1$ (where m_X^2 denotes the squared effective mass of the unobserved particles[3]), has been tested at an incident proton momentum of 6 GeV/c (Ref. 4). In this experiment, we have conducted a further test of this model at 11.75 GeV/c, and we have compiled inclusive data for meson final states and deuteron targets.

Although we presently know of no theoretical models for these latter reactions, it is important to note that even at these energies, the spin effects are not small and that the data show a consistent phenomenological structure, which must be explainable by a comprehensive model of inclusive strong interactions. In this paper, we shall elucidate these phenomenological features as well as compare the predictions of the existing inclusive proton production models with the experimental data. The plan of this paper is as follows: the next section describes the experimental method in some detail. Section III discusses the features of the measured data. In Sec. IV, we summarize the recurrent patterns in the data and discuss the relevant existent models, including the triple-Regge treatment of inclusive proton production.

II. METHOD

The experiment, performed in the extracted polarized beam of the ZGS, is diagrammed in Fig. 1. The beam, after passing through a thin polyethylene polarization monitor, entered a 10-cm-long, 3.8-cm-diameter liquid hydrogen (or deuterium) target. Particles produced (to the left) at the selected angle (0 to 17°) and momentum (2 to 9 GeV/c) were deflected by dipoles

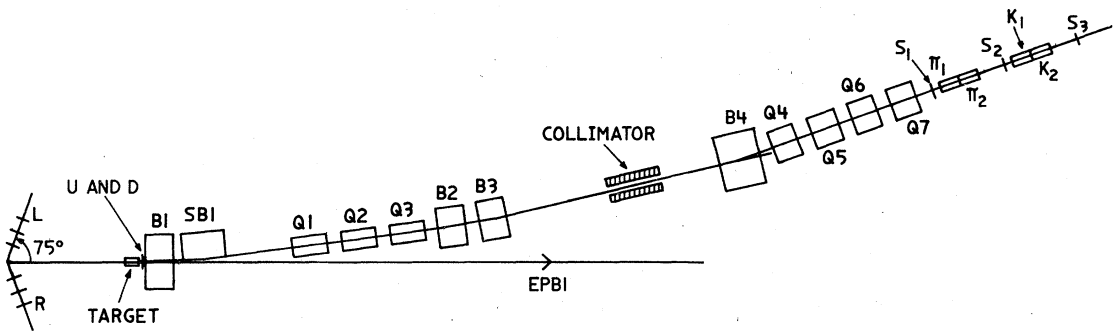

FIG. 1. Plan view of the experiment.

$B1$ and $SB1$ to the axis of quadrupoles $Q1-3$, and further deflected by $B2-3$ toward an intermediate (momentum) focus.

A collimator at this position accepted particles in a momentum bite $\Delta p/p = \pm 5\%$. This acceptance, along with the $\pm 0.25°$ angular acceptance of $Q1$, determined the resolution in the various kinematic variables. After a further bend and momentum recombination, the particles were detected by three scintillation counters $S1-3$.

The Cherenkov detectors π_1, π_2, K_1, and K_2 were filled with ethylene gas and were capable of complete separation of π (and μ, e), K and p events in the momentum range 3–9 GeV/c. Although the two π (and K) counters shared common pressure vessels, they were optically isolated and each segment was viewed by an independent RCA4522 photomultiplier tube. This arrangement minimized the possible contamination of the small K^+ signal due to δ-ray production by the copious proton flux that was observed. A pion was defined as a coincidence between $S1-3$ and $\pi 1-2$; a kaon by $S1-3$, $K1-2$, and the absence of both $\pi 1$ and $\pi 2$, and a proton by $S1-3$, with no Cherenkov coincident. A small number (<1%) of $S1-3$ coincidences met none of these criteria, and were ignored.

The incident protons were polarized in the vertical direction, normal to the scattering plane. The polarization direction was reversed after every accelerator pulse, in order to minimize the systematic errors in the experiment. The direction, size, and position of the incident beam were monitored by two sets of x-y proportional chambers (not shown in Fig. 1) whose signals were integrated over the 0.5-sec duration of the ZGS spill. The relative intensity (typically 5×10^8 polarized protons per spill) and polarization (typically 50%) were monitored by a set of two three-counter telescopes set at angles of 75° to the left (L) and right (R) of the beam direction, which viewed a thin polyethylene target. The target was much larger than the size of the beam. The analyzing power of this polarimeter, while diluted by inelastic reactions and by the other constituents in the polyethylene, was calibrated against an absolute proton-elastic-scattering polarimeter located in a branch of the extracted beam immediately upstream of this experiment.[5] The analyzing power was $A_a = 0.0207 \pm 0.0010$. The beam polarization was then calculated from the expression[6]

$$P_B = \frac{L_\uparrow + R_\downarrow - L_\downarrow - R_\uparrow}{IA_a}$$

summed over an experimental run, where $I = L_\uparrow + R_\uparrow + L_\downarrow + R_\downarrow$ is a relative measure of the intensity of the extracted beam. ($L_\uparrow$, for example, denotes the number of coincidences in the left polarimeter arm with the incident beam polarized up.)

A secondary set of two telescopes (U and D in Fig. 1) viewed the target in the vertical plane, again at angles of approximately 75°. These telescopes monitored the stability of the closed, self-refrigerating target, provided a useful check on the intensity determination and, incidentally, provided evidence that the horizontal component of the beam polarization was unobservably small.

A significant check on possible systematic errors (particularly in the determination of the analyzing power of the polarimeter) was performed in an earlier experiment with the same equipment at an incident momentum of 6 GeV/c. At this momentum we were able to measure the asymmetry for proton-proton elastic scattering, which must equal the (well-measured) polarization parameter. The data obtained were entirely consistent with previous measurements.[7]

This spectrometer was not designed for the experiment, but as a secondary beam line which combined high resolution, large acceptance, and the capability of attaining zero-degree production for negative beams. The flexibility of this design

was exploited, but the limited bending power of the dipoles involved implied a set of limitations on the momentum and laboratory angles that could be achieved. (Radiation safety considerations eliminated small production angles for positive particles.) These limitations were partially offset by allowing the scattered particles to pass through quadrupoles $Q1-3$ off axis and then restoring with dipoles $B2-3$.

The majority of the data were taken with the spectrometer in the unaltered mode, where the acceptance was determined by the 5% momentum bite at the intermediate focus and the ±0.25 degree aperture of $Q1$. The acceptance in the expanded mode varied from point to point and was less than the unaltered value by factors ranging from 1.2 to 3.0. The exact value of the acceptance of the spectrometer under these conditions was difficult to calculate: cross sections derived from these data were consistent with those of Ref. 1, but are not as reliable. Whenever cross-section data are utilized in this paper (Sec. IV, below) they are taken from Ref. 1. Because of the rapid reversal of the incident polarization direction, possible long-term drifts in the size of the acceptance had no effect on the asymmetry measurements. There was no evidence of changes in the acceptance size which were correlated with the incident beam polarization.

Even with this expanded angular coverage, the range of data presented here is limited. For positive particles, data were obtained for momentum transfers $(t-t_{\min})$ between 0.08 and 1.7 $(\mathrm{GeV}/c)^2$. The data for negative particles extended from 0.01 to 1.0 $(\mathrm{GeV}/c)^2$.

The inclusive asymmetries were obtained from the equation

$$A=\frac{1}{P_B}\,\frac{N_\uparrow-N_\downarrow}{N_\uparrow+N_\downarrow},$$

where $N_\uparrow$ ($N_\downarrow$) is the number of detected particles of the appropriate type with beam polarization up (down) normalized to the incident intensity and with target-empty corrections (approximately 15%) applied. The asymmetry defined above is positive when more particles are produced to the left with incident beam polarization up. This definition is a natural extension of the Basel convention for elastic-scattering polarized-target experiments.

Some data from this experiment taken with a liquid hydrogen target (along with data taken at 6 GeV/c incident momentum) have been presented previously in graphical form.[8] Tables I and II contain π^+ and π^- production from hydrogen, along with data taken with a deuterium target. Tables III–V present data on K^+, K^-, and proton production.

The kinematic variables provided in Tables I–V are the square of the four-momentum transfer from the incoming proton to the produced particle (called u for meson production and t for proton production) and x, the ratio of the longitudinal momentum in the center-of-mass system to the maximum value it can attain. For consistency, all x values are calculated assuming that the target is hydrogen. This variable is, over the range covered by the data, roughly proportional to the laboratory momentum of the produced particle. The data were taken at fixed secondary momenta, i.e., at approximately fixed x. The momentum transfer was selected as the relevant angular variable after inspecting the data; the location of zeros, for example, seems to be approximately constant in this variable over a wide range in x. This stability would not be the case if p_T, the transverse component of the momentum, had been selected as the angular variable. The change in nomenclature from t to u reflects our conjecture that different exchange mechanisms dominate the structure of the data; meson exchange for proton production and baryon exchange for meson production.

The tables also include the deuterium-target asymmetry and the derived asymmetry for production from a neutron target. The neutron-target data were calculated by a simple deuterium-hydrogen subtraction which included target-empty, beam-polarization, and density corrections, and a further small correction for the shadowing of the proton by the neutron. These are only the obvious corrections—there are effects introduced by the exchange of pions that create a part of the binding potential which can contribute to the observed asymmetry in pion production by deuterium, for example. Thus we caution the reader that the tabulated neutron-target asymmetries must be regarded as approximate.

The errors quoted in the tables include a 5% uncertainty in our knowledge of the analyzing power of the polarimeter, statistical errors, and, in the case of neutron-target asymmetries, an additional 5% uncertainty in the density/shadowing correction, all taken in quadrature. The resolution in u (or t) and x varies somewhat over the kinematic range surveyed. At low t the resolution is approximately ±0.03 $(\mathrm{GeV}/c)^2$ full width at half maximum (FWHM). This increases, linearly, to ±0.10 $(\mathrm{GeV}/c)^2$ at $-t=1.0$ $(\mathrm{GeV}/c)^2$. The resolution in x varies from ±0.02 at $x=0.2$ to ±0.04 at $x=0.8$.

TABLE I. Asymmetries for inclusive π^+ production. Tabulated are the spectrometer settings p_{1ab} and θ_{1ab}, the derived kinematical quantities $u=(p_{in}-p_\pi)^2$ and $x=p_l/p_{l,\,max}$, the left-right production asymmetry for a hydrogen target A_h and for a deuterium target A_d, and the derived asymmetry for the neutron target A_n. The errors include statistics and an estimate of possible systematic effects.

p_{1ab} (GeV/c)	θ_{1ab} (deg)	u [(GeV/c)^2]	x	A_h	A_d	A_n
2	9.0	0.06	0.15	−0.044 ± 0.010		
	11.3	−0.27	0.14	−0.010 ± 0.016		
	15.0	−0.97	0.10	−0.048 ± 0.038		
	17.0	−1.42	0.08	0.010 ± 0.045		
3	6.9	0.09	0.25	−0.035 ± 0.007		
	8.8	−0.22	0.24	−0.007 ± 0.010		
4	2.6	0.45	0.37	−0.024 ± 0.009	−0.021 ± 0.006	−0.019 ± 0.015
	4.1	0.31	0.36	−0.029 ± 0.011	−0.036 ± 0.007	−0.046 ± 0.018
	5.8	0.06	0.35	−0.057 ± 0.011	−0.050 ± 0.008	−0.041 ± 0.021
	7.2	−0.21	0.34	−0.026 ± 0.010	−0.045 ± 0.024	−0.069 ± 0.054
	8.2	−0.43	0.33	0.018 ± 0.017	0.027 ± 0.009	0.039 ± 0.030
	8.8	−0.56	0.33	0.061 ± 0.014	0.050 ± 0.010	0.035 ± 0.028
5	2.6	0.36	0.46	−0.020 ± 0.006	−0.036 ± 0.006	−0.055 ± 0.014
	3.8	0.23	0.46	−0.040 ± 0.013		
	5.1	0.01	0.45	−0.050 ± 0.014		
	6.3	−0.23	0.44	−0.019 ± 0.013		
	7.1	−0.42	0.44	0.043 ± 0.012		
	7.6	−0.54	0.43	0.073 ± 0.020	0.065 ± 0.010	0.054 ± 0.035
6	2.6	0.27	0.55	−0.010 ± 0.006	−0.015 ± 0.004	−0.023 ± 0.011
	3.6	0.14	0.55	−0.039 ± 0.011		
	4.7	−0.06	0.55	−0.045 ± 0.013		
	5.7	−0.28	0.54	0.011 ± 0.012		
	6.3	−0.45	0.54	0.046 ± 0.014		
	6.7	−0.56	0.54	0.061 ± 0.014	0.061 ± 0.011	0.059 ± 0.035
6.5	4.5	−0.10	0.60	−0.056 ± 0.011		
7	2.6	0.18	0.65	−0.006 ± 0.008	−0.013 ± 0.005	−0.025 ± 0.017
	3.4	0.05	0.65	−0.065 ± 0.016	−0.040 ± 0.008	−0.001 ± 0.028
	4.4	−0.14	0.65	−0.071 ± 0.013	−0.051 ± 0.012	0.069 ± 0.099
	5.2	−0.34	0.64	−0.004 ± 0.014	0.020 ± 0.008	0.060 ± 0.028
	5.9	−0.54	0.64	0.084 ± 0.024	0.074 ± 0.012	0.059 ± 0.046
	6.4	−0.67	0.64	0.078 ± 0.020	0.122 ± 0.016	0.195 ± 0.049
	7.5	−1.06	0.64	0.159 ± 0.017		
	8.0	−1.26	0.64	0.213 ± 0.041		
7.5	1.7	0.23	0.70	−0.016 ± 0.005		
	2.6	0.13	0.70	−0.049 ± 0.010		
	3.4	0.01	0.70	−0.077 ± 0.026		
	4.3	−0.18	0.70	−0.065 ± 0.013		
	5.3	−0.43	0.70	0.050 ± 0.019		
	5.9	−0.62	0.70	0.179 ± 0.026		
	7.5	−1.20	0.70	0.163 ± 0.031		
	8.0	−1.41	0.70	0.245 ± 0.048		
8	2.6	0.09	0.74	−0.139 ± 0.018	−0.111 ± 0.012	−0.055 ± 0.045
	3.3	−0.03	0.75	−0.154 ± 0.015	−0.131 ± 0.010	−0.101 ± 0.023
	4.2	−0.23	0.75	−0.048 ± 0.014		
	4.5	−0.31	0.75	−0.049 ± 0.023	0.036 ± 0.011	0.157 ± 0.039
	5.3	−0.52	0.75	0.118 ± 0.030	0.148 ± 0.025	0.212 ± 0.092
	5.9	−0.71	0.75	0.244 ± 0.037	0.257 ± 0.026	0.279 ± 0.085
	6.3	−0.85	0.75	0.229 ± 0.033	0.321 ± 0.034	0.470 ± 0.094
	7.3	−1.23	0.76	0.319 ± 0.050		
	7.8	−1.44	0.76	0.331 ± 0.061		

TABLE I. (*Continued*)

p_{lab} (GeV/c)	θ_{lab} (deg)	u [(GeV/c)^2]	x	A_h	A_d	A_n
8.5	2.2	0.09	0.79	−0.116 ± 0.013	−0.122 ± 0.014	−0.133 ± 0.044
	2.6	0.04	0.79	−0.155 ± 0.021	−0.118 ± 0.011	−0.036 ± 0.052
	3.3	−0.09	0.79	−0.098 ± 0.016		
	4.3	−0.32	0.80	0.086 ± 0.031		
	5.2	−0.58	0.80	0.297 ± 0.041		
	6.2	−0.94	0.81	0.382 ± 0.050		
	7.5	−1.47	0.82	0.329 ± 0.058		
9	2.6	−0.01	0.84	−0.092 ± 0.031	−0.084 ± 0.021	−0.065 ± 0.058
	3.5	−0.19	0.85	−0.042 ± 0.030		
	4.3	−0.40	0.85	0.197 ± 0.032	0.248 ± 0.026	0.432 ± 0.137
	5.2	−0.67	0.86	0.394 ± 0.047		
	6.2	−1.02	0.87	0.402 ± 0.077	0.533 ± 0.057	0.736 ± 0.161

TABLE II. Asymmetries for inclusive π^- production. Tabulated are the spectrometer settings p_{lab} and θ_{lab}, the derived kinematical quantities $u=(p_{1n}-p_\pi)^2$ and $x=p_l/p_{l,\,max}$, the left-right production asymmetry for a hydrogen target A_h and for a deuterium target A_d, and the derived asymmetry for the neutron target A_n. The errors include statistics and an estimate of possible systematic effects.

p_{lab} (GeV/c)	θ_{lab} (deg)	u [(GeV/c)^2]	x	A_h	A_d	A_n
1.5	2.6	0.60	0.13	−0.001 ± 0.026		
3	2.6	0.53	0.28	0.040 ± 0.012	0.018 ± 0.005	0.003 ± 0.009
4	2.6	0.45	0.38	0.055 ± 0.009	0.051 ± 0.008	0.048 ± 0.017
5	2.6	0.36	0.47	0.065 ± 0.012	0.057 ± 0.007	0.050 ± 0.015
	4.0	0.19	0.47	0.097 ± 0.016		
	4.5	0.12	0.47	0.088 ± 0.017		
	6.0	−0.16	0.46	0.051 ± 0.036		
6	2.6	0.27	0.57	0.180 ± 0.021	0.222 ± 0.024	0.259 ± 0.044
	3.5	0.15	0.57	0.147 ± 0.017		
	4.5	−0.02	0.56	0.044 ± 0.014		
	5.5	−0.24	0.56	0.049 ± 0.018		
	6.5	−0.49	0.55	0.176 ± 0.073		
7	0.7	0.33	0.67	0.162 ± 0.015		
	1.0	0.32	0.67	0.231 ± 0.023		
	2.6	0.18	0.67	0.160 ± 0.013		
	3.5	0.04	0.67	0.047 ± 0.008		
	4.5	−0.16	0.66	−0.035 ± 0.014		
	5.3	−0.35	0.66	0.068 ± 0.018		
	5.8	−0.48	0.66	0.084 ± 0.023		
7.5	0.8	0.29	0.72	0.311 ± 0.063	0.227 ± 0.028	0.158 ± 0.068
	2.6	0.13	0.72	0.151 ± 0.015		
	3.3	0.02	0.72	0.040 ± 0.020		
8	0.6	0.26	0.76	0.194 ± 0.021		
	0.9	0.25	0.76	0.252 ± 0.020		
	2.6	0.09	0.77	0.183 ± 0.025		
	3.5	−0.08	0.77	0.009 ± 0.027		
	4.0	−0.19	0.77	−0.097 ± 0.028		
	4.5	−0.31	0.77	−0.130 ± 0.033		
	5.0	−0.44	0.77	−0.018 ± 0.024		
	5.5	−0.59	0.77	0.002 ± 0.039		
	6.0	−0.76	0.77	0.050 ± 0.047		

TABLE II. (*Continued*)

p_{lab} (GeV/c)	θ_{lab} (deg)	u [(GeV/c)^2]	x	A_h	A_d	A_n
8.5	1.0	0.20	0.81	0.347 ± 0.068	0.267 ± 0.030	0.216 ± 0.058
	2.6	0.04	0.81	0.216 ± 0.033	0.251 ± 0.022	0.268 ± 0.033
	3.0	−0.04	0.82	0.046 ± 0.032	0.167 ± 0.022	0.221 ± 0.031
	3.5	−0.14	0.82	−0.080 ± 0.037	0.041 ± 0.020	0.103 ± 0.031
	4.3	−0.31	0.82	−0.056 ± 0.039	−0.044 ± 0.022	−0.038 ± 0.034
9	1.1	0.16	0.86	0.306 ± 0.035		
	2.6	−0.01	0.86	0.071 ± 0.043		
	3.5	−0.19	0.87	−0.137 ± 0.050		
	4.5	−0.45	0.88	−0.148 ± 0.091		

TABLE III. Asymmetries for inclusive K^+ production. Tabulated are the spectrometer settings p_{lab} and θ_{lab}, the derived kinematical quantities $u=(p_{in}-p_K)^2$ and $x=p_l/p_{l,\,max}$, the left-right production asymmetry for a hydrogen target A_h and for a deuterium target A_d, and the derived asymmetry for the neutron target A_n. The errors include statistics and an estimate of possible systematic effects.

p_{lab} (GeV/c)	θ_{lab} (deg)	u [(GeV/c)^2]	x	A_h	A_d	A_n
3	6.9	−0.56	0.22	−0.06 ± 0.04		
	8.8	−0.87	0.21	0.06 ± 0.06		
4	2.6	0.02	0.35	0.12 ± 0.06	0.03 ± 0.03	−0.06 ± 0.07
	4.1	−0.13	0.35	0.05 ± 0.05	0 ± 0.03	−0.07 ± 0.07
	5.8	−0.37	0.34	0.03 ± 0.04	−0.03 ± 0.03	−0.09 ± 0.06
	7.2	−0.64	0.33	0.04 ± 0.04	0.01 ± 0.09	−0.04 ± 0.21
	8.2	−0.86	0.32	−0.10 ± 0.08	0.04 ± 0.04	0.19 ± 0.12
	8.8	−1.00	0.31	0.02 ± 0.06	0 ± 0.04	−0.02 ± 0.10
5	2.6	0.06	0.46	0.08 ± 0.02	0.05 ± 0.02	0.01 ± 0.04
	3.8	−0.08	0.45	0.01 ± 0.05		
	5.1	−0.30	0.45	0.11 ± 0.05		
	6.3	−0.53	0.44	0.10 ± 0.06		
	7.1	−0.72	0.43	0.01 ± 0.05		
	7.6	−0.84	0.43	0.21 ± 0.09	0.06 ± 0.04	−0.10 ± 0.11
6	2.6	0.06	0.56	0.04 ± 0.02	0.03 ± 0.02	0.04 ± 0.04
	3.6	−0.07	0.56	0.11 ± 0.04		
	4.7	−0.28	0.55	0.17 ± 0.05		
	5.7	−0.49	0.55	0.19 ± 0.05		
	6.3	−0.66	0.55	0.09 ± 0.06		
	6.7	−0.77	0.54	0.13 ± 0.06	0.09 ± 0.04	0.04 ± 0.10
6.5	4.5	−0.28	0.61	0.12 ± 0.04		
7	2.6	0.03	0.66	0.11 ± 0.04	0.02 ± 0.02	−0.08 ± 0.06
	3.4	−0.10	0.66	0.14 ± 0.06	0.08 ± 0.03	0 ± 0.09
	4.4	−0.29	0.66	0.11 ± 0.05	0.13 ± 0.05	0.25 ± 0.23
	5.2	−0.49	0.66	0.10 ± 0.06	0.12 ± 0.03	0.14 ± 0.08
	5.9	−0.69	0.66	0.23 ± 0.09	0.24 ± 0.04	0.26 ± 0.13
	6.4	−0.83	0.66	0.15 ± 0.08	0.05 ± 0.05	−0.07 ± 0.12
	7.5	−1.22	0.66	0.12 ± 0.05		
	8.0	−1.41	0.66	0.01 ± 0.13		
7.5	1.7	0.10	0.71	0.02 ± 0.02		
	3.4	−0.12	0.72	0.08 ± 0.08		
	5.3	−0.56	0.72	0.22 ± 0.08		
	5.9	−0.75	0.72	0.24 ± 0.08		
	7.5	−1.33	0.72	0.11 ± 0.11		
	8.0	−1.53	0.72	0.15 ± 0.17		

TABLE III. (*Continued*)

p_{lab} (GeV/c)	θ_{lab} (deg)	u [(GeV/c)^2]	x	A_h	A_d	A_n
8	2.6	−0.02	0.77	0.10 ± 0.04	0.07 ± 0.02	0.02 ± 0.06
	3.3	−0.14	0.77	0.13 ± 0.03	0.09 ± 0.02	0.06 ± 0.03
	4.5	−0.41	0.77	0.19 ± 0.08	0.16 ± 0.04	0.12 ± 0.09
	5.3	−0.62	0.77	0.17 ± 0.10	0.19 ± 0.06	0.23 ± 0.17
	5.9	−0.82	0.78	0.03 ± 0.10	0.20 ± 0.05	0.38 ± 0.15
	6.3	−0.95	0.78	0.17 ± 0.10	0.29 ± 0.07	0.42 ± 0.16
	7.3	−1.34	0.79	−0.03 ± 0.14		
	7.8	−1.55	0.79	0.31 ± 0.18		
8.5	2.2	0.01	0.82	0.07 ± 0.03	0.03 ± 0.02	−0.03 ± 0.06
	2.6	−0.05	0.82	0.12 ± 0.04	0.07 ± 0.02	0.02 ± 0.05
	3.3	−0.17	0.82	0.06 ± 0.04		
	4.3	−0.40	0.83	0.21 ± 0.09		
	5.2	−0.67	0.83	0.26 ± 0.12		
	6.2	−1.02	0.84	0.33 ± 0.13		
	7.5	−1.56	0.86	0.21 ± 0.15		
9	2.6	−0.08	0.87	0.35 ± 0.19	0.06 ± 0.04	0 ± 0.04
	3.5	−0.26	0.88	0.19 ± 0.09		
	4.3	−0.47	0.88	0.08 ± 0.09	0.12 ± 0.05	0.16 ± 0.10
	5.2	−0.74	0.89	0.09 ± 0.11		
	6.2	−1.09	0.91	0.12 ± 0.19	0.17 ± 0.11	0.24 ± 0.27

TABLE IV. Asymmetries for inclusive K^- production. Tabulated are the spectrometer settings p_{lab} and θ_{lab}, the derived kinematical quantities $u=(p_{in}-p_K)^2$ and $x=p_l/p_{l,\,max}$, the left-right production asymmetry for a hydrogen target A_h and for a deuterium target A_d, and the derived asymmetry for the neutron target A_n. The errors include statistics and an estimate of possible systematic effects.

p_{lab} (GeV/c)	θ_{lab} (deg)	u [(GeV/c)^2]	x	A_h	A_d	A_n
3	2.6	−0.12	0.26	−0.12 ± 0.14	0.03 ± 0.06	0.11 ± 0.09
4	2.6	0.02	0.38	−0.06 ± 0.07	0.07 ± 0.05	0.20 ± 0.12
5	2.6	0.06	0.49	0.02 ± 0.10	0.01 ± 0.05	0.03 ± 0.11
	4.0	−0.11	0.49	0.17 ± 0.11		
	4.5	−0.19	0.49	−0.10 ± 0.13		
6	2.6	0.06	0.60	0.07 ± 0.12	0.24 ± 0.08	0.41 ± 0.18
	3.5	−0.07	0.60	0.11 ± 0.09		
	4.5	−0.24	0.60	0.29 ± 0.16		
	5.5	−0.45	0.60	0.26 ± 0.19		
7	0.7	0.18	0.72	0.14 ± 0.09		
	1.0	0.16	0.72	0.46 ± 0.12		
	2.6	0.03	0.72	0.32 ± 0.11		
	3.5	−0.12	0.72	0.18 ± 0.14		
	4.5	−0.32	0.72	0.37 ± 0.22		
	5.3	−0.50	0.72	0.60 ± 0.37		
7.5	2.6	0.01	0.77	0.57 ± 0.19		
8	0.9	0.14	0.82	0.56 ± 0.20		

TABLE V. Asymmetries for inclusive proton production. Tabulated are the spectrometer settings p_{lab} and θ_{lab}, the derived kinematical quantities $t=(p_{in}-p_p)^2$ and $x=p_l/p_{l,\,max}$, the left-right production asymmetry for a hydrogen target A_h and for a deuterium target A_d, and the derived asymmetry for the neutron target A_n. The errors include statistics and an estimate of possible systematic effects.

p_{lab} (GeV/c)	θ_{lab} (deg)	t [(GeV/c)^2]	x	A_h	A_d	A_n
2	9.0	−3.90	−0.07	0.005 ± 0.011		
	11.3	−4.22	−0.09	0.020 ± 0.022		
	15.0	−4.92	−0.12	−0.054 ± 0.044		
	17.0	−5.37	−0.15	−0.031 ± 0.052		
3	6.9	−2.35	0.09	0.012 ± 0.007		
	8.8	−2.66	0.07	0.006 ± 0.011		
4	2.6	−1.19	0.23	−0.014 ± 0.009	−0.008 ± 0.005	−0.002 ± 0.012
	4.1	−1.33	0.22	0 ± 0.008	−0.006 ± 0.005	−0.013 ± 0.012
	5.8	−1.58	0.21	0.016 ± 0.007	0.016 ± 0.004	0.016 ± 0.011
	7.2	−1.85	0.20	0.019 ± 0.007		
	8.2	−2.07	0.19	0.018 ± 0.012	0.025 ± 0.007	0.033 ± 0.019
	8.8	−2.20	0.19	0.004 ± 0.009	0.012 ± 0.006	0.022 ± 0.015
5	2.6	−0.79	0.34	−0.012 ± 0.004	−0.011 ± 0.003	−0.011 ± 0.008
	3.8	−0.92	0.33	−0.014 ± 0.007		
	5.1	−1.14	0.32	0.020 ± 0.007		
	6.3	−1.38	0.32	0.023 ± 0.007		
	7.1	−1.57	0.31	0.021 ± 0.006		
	7.6	−1.69	0.30	0.030 ± 0.010	0.010 ± 0.005	−0.014 ± 0.015
6	2.6	−0.55	0.44	0.002 ± 0.003	0.005 ± 0.002	0.009 ± 0.006
	3.6	−0.68	0.43	0.008 ± 0.005		
	4.7	−0.88	0.43	0.006 ± 0.005		
	5.7	−1.10	0.42	0.013 ± 0.005		
	6.3	−1.27	0.42	0.010 ± 0.005		
	6.7	−1.38	0.42	0.002 ± 0.006	−0.001 ± 0.004	−0.004 ± 0.011
6.5	4.5	−0.79	0.48	0.007 ± 0.004		
7	2.6	−0.40	0.54	0.019 ± 0.004	0.010 ± 0.003	−0.003 ± 0.008
	3.4	−0.53	0.53	0.033 ± 0.008	0.014 ± 0.003	−0.010 ± 0.012
	4.4	−0.72	0.53	0.014 ± 0.004	0.014 ± 0.004	0.013 ± 0.019
	5.2	−0.92	0.53	0.008 ± 0.005	−0.006 ± 0.003	−0.024 ± 0.008
	5.9	−1.12	0.52	0.016 ± 0.007	−0.006 ± 0.003	−0.031 ± 0.011
	6.4	−1.26	0.52	0.017 ± 0.006	−0.003 ± 0.003	−0.029 ± 0.010
	7.5	−1.65	0.51	0.022 ± 0.004		
	8.0	−1.84	0.51	0.012 ± 0.008		
7.5	1.7	−0.26	0.59	0.021 ± 0.002		
	2.6	−0.35	0.58	0.024 ± 0.004		
	3.4	−0.48	0.58	0.027 ± 0.006		
	4.3	−0.67	0.58	0.017 ± 0.004		
	5.3	−0.92	0.58	0.007 ± 0.005		
	5.9	−1.11	0.57	0.017 ± 0.005		
	7.5	−1.69	0.57	0.010 ± 0.006		
	8.0	−1.89	0.56	0.018 ± 0.008		
8	2.6	−0.32	0.63	0.035 ± 0.005	0.025 ± 0.003	0.009 ± 0.010
	3.3	−0.44	0.63	0.032 ± 0.003	0.027 ± 0.002	0.023 ± 0.004
	4.2	−0.63	0.63	0.022 ± 0.004		
	4.5	−0.71	0.63	0.021 ± 0.005	0.017 ± 0.003	0.014 ± 0.007
	5.3	−0.92	0.63	0.019 ± 0.006	0.007 ± 0.004	−0.008 ± 0.011
	5.9	−1.12	0.63	0 ± 0.006	0.008 ± 0.003	−0.024 ± 0.010
	6.3	−1.25	0.63	0.019 ± 0.005	0.009 ± 0.004	−0.002 ± 0.009
	7.3	−1.63	0.62	0.028 ± 0.006		
	7.8	−1.85	0.62	0.038 ± 0.008		

TABLE V. (*Continued*)

p_{lab} (GeV/c)	θ_{lab} (deg)	t [(GeV/c)^2]	x	A_h	A_d	A_n
8.5	2.2	−0.24	0.68	0.038 ± 0.004	0.035 ± 0.004	0.030 ± 0.009
	2.6	−0.29	0.68	0.037 ± 0.005	0.031 ± 0.003	0.020 ± 0.009
	3.6	−0.42	0.68	0.033 ± 0.004		
	4.3	−0.65	0.68	0.044 ± 0.007		
	5.2	−0.91	0.68	0.032 ± 0.006		
	6.2	−1.27	0.68	0.053 ± 0.006		
	7.5	−1.80	0.68	0.035 ± 0.006		
9	2.6	−0.27	0.73	0.043 ± 0.006	0.038 ± 0.004	0.030 ± 0.012
	3.5	−0.46	0.73	0.048 ± 0.006		
	4.3	−0.67	0.73	0.038 ± 0.004	0.025 ± 0.003	0.001 ± 0.010
	5.2	−0.94	0.73	0.048 ± 0.005		
	6.2	−1.29	0.73	0.036 ± 0.007	0.011 ± 0.004	−0.015 ± 0.009

III. RESULTS

A. π^+ production

Figure 2 presents the asymmetry from hydrogen for two values of the momentum transfer, $u = 0$ and -0.5 (GeV/c)^2, as a function of x. Both sets of data show an increase of the magnitude of the asymmetry at high x beginning in the region $x = 0.7$. There is no indication of any x dependence below $x = 0.55$.

Representative data from Table I for a hydrogen target are shown in Figs. 3(a) and 4(a) as a function of u, for $x > 0.7$ and $x < 0.7$, respectively. Note the difference in both the vertical scale, due to the x dependence, and the horizontal scale, due to the limitations on the accessible kinematic region. Both sets of data show asymmetries that are negative in the region $u > -0.2$ (GeV/c)^2, and positive thereafter. For the highest x values and momentum transfers, these asymmetries are large. There is a minimum in the region near $u = 0$ (less distinct at low x) and a crossover to

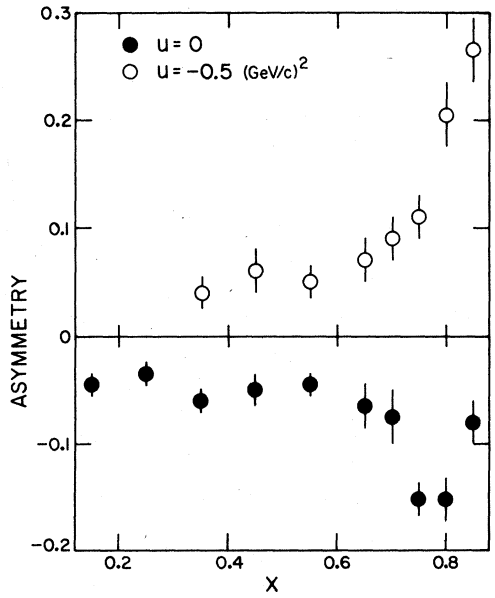

FIG. 2. The asymmetry for inclusive π^+ production from hydrogen at fixed $u = 0$ and -0.5 (GeV/c)^2 as a function of the scaling variable x.

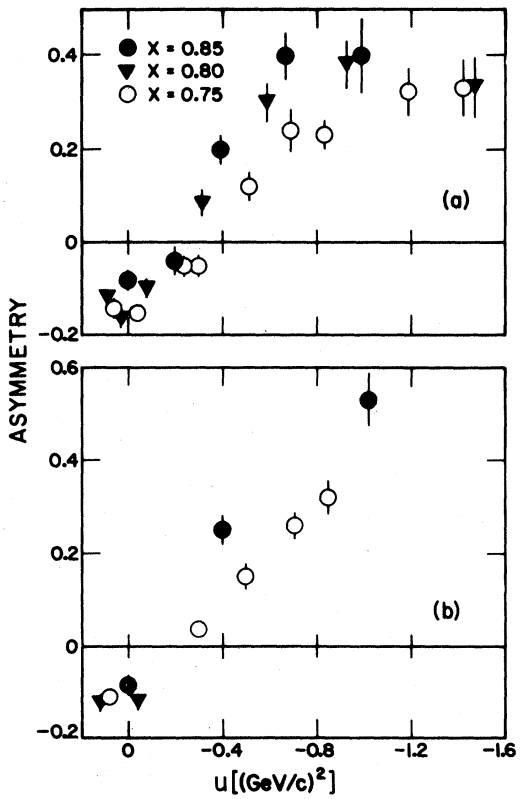

FIG. 3. The asymmetry for inclusive π^+ production at large x from (a) hydrogen and (b) deuterium targets. (The deuteron is treated as a proton for the assignment of x).

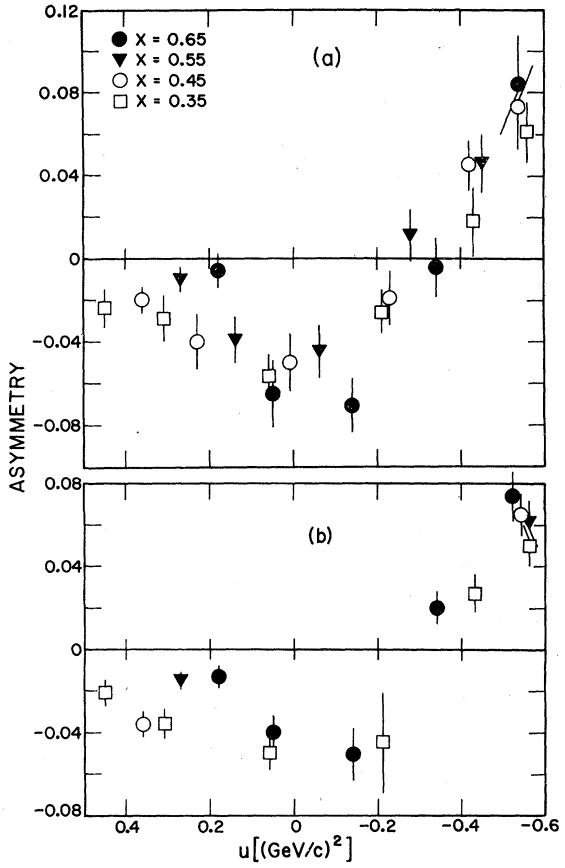

FIG. 4. The asymmetry for inclusive π^+ production at small x from (a) hydrogen and (b) deuterium targets.

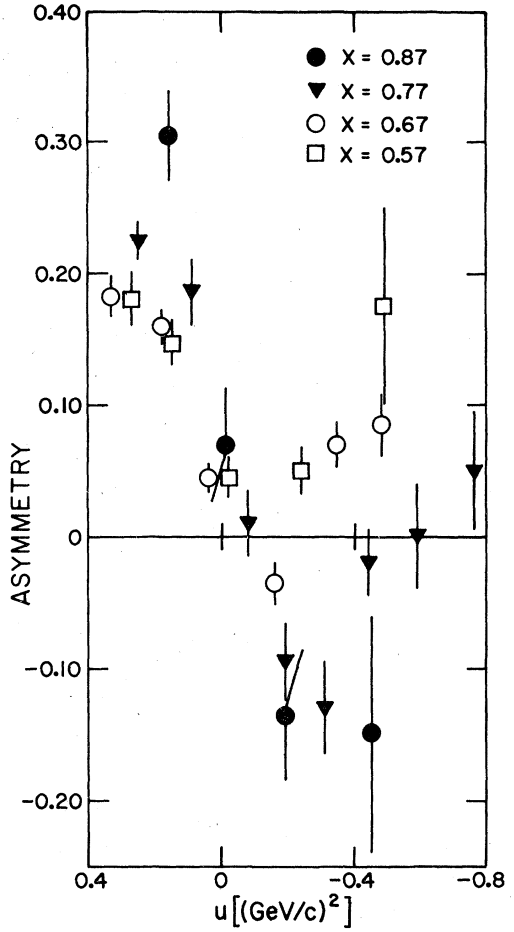

FIG. 5. The asymmetry for inclusive π^- production from hydrogen.

positive asymmetry near $u = -0.3$ (GeV/c)^2. This structure is present at all values of x, and is striking at the largest values.

The data obtained from a deuterium target are shown in Figs. 3(b) and 4(b). The data are entirely consistent with the hydrogen data. The cross sections for production from deuterium are approximately double those from hydrogen, so that the derived production asymmetry from the neutron in deuterium is well determined and equal to that of the proton.

B. π^- production

The asymmetry for production of π^- mesons is shown in Fig. 5 for several values of x as a function of u. There is, again, considerable structure in the data. The asymmetry is positive for positive u, and falls toward a zero at $u = -0.1$ (GeV/c)^2. After attaining a minimum in the region between u values of -0.1 and -0.4, the asymmetry then increases. This structure is x dependent (in contrast to π^+ production): the minimum both broadens and deepens as x increases. At the lowest x shown, $x = 0.57$, the asymmetry remains positive over the entire u region surveyed.

The data in Table II for very small angles at x values of 0.67 and 0.77 have been combined in Fig. 5, but the detailed data are interesting. The asymmetry rises from zero in the forward direction very quickly: at $x = 0.77$ it is very nearly at its maximum just 0.6° from the forward direction. This angle corresponds to a $u' = u - u_{\max}$ of -0.007 (GeV/c)^2, more than an order of magnitude smaller than the maximum asymmetry point for forward proton-proton elastic scattering.

The x dependence of the asymmetry is shown in Fig. 6, where the extrapolated values at fixed u are plotted. There is an apparent divergence from a small positive value (+0.05) that is approximately linear in x over the range shown. The data in Table II that exist below $x = 0.47$ are consistent with this feature. This behavior is strikingly different from the behavior of the π^+ data in Fig. 2.

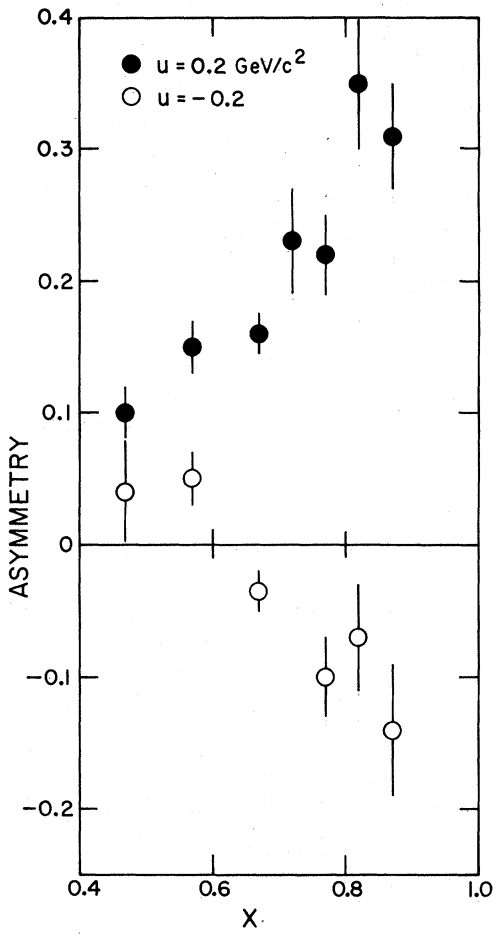

FIG. 6. The asymmetry for inclusive π^- production from hydrogen at fixed $u = \pm 0.2$ $(\mathrm{GeV}/c)^2$ as a function of x.

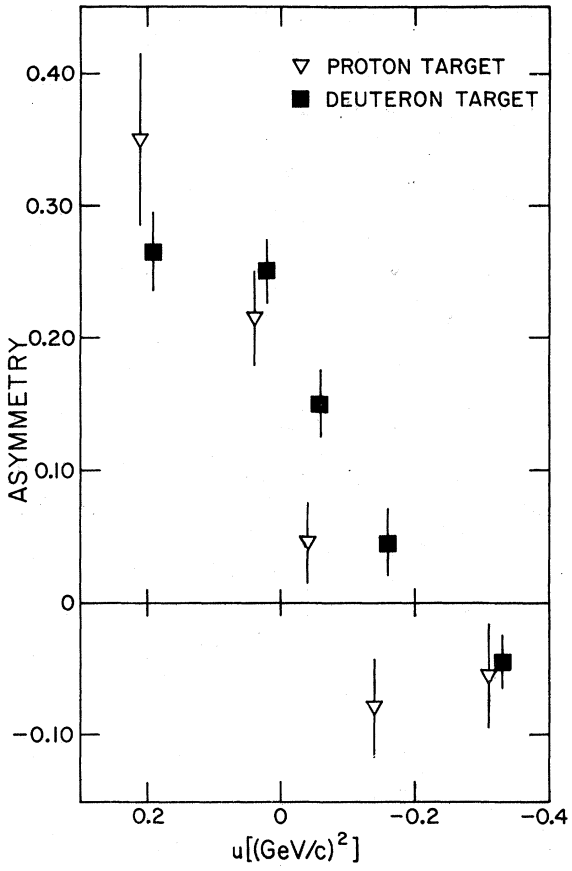

FIG. 7. Comparison between inclusive π^- production from hydrogen and deuterium targets at $x = 0.82$. The deuterium points are slightly displaced for clarity.

Few data were obtained with a deuterium target. The results of the only extended data set are presented in Fig. 7, together with the corresponding hydrogen data. As in the case of π^+ production, the two sets of data are in substantial agreement. Thus the inclusive production of pions seems to be independent of the isospin coordinate of the target particle.

C. K^+ production

The data on the production of positive kaons is shown in Fig. 8. The data from Table III have been combined into three x ranges, 0.21–0.46, 0.54–0.72, and 0.77–0.91, in order to increase the statistical significance of the displayed data. Except in the positive u region, the data are consistent with a flat dependence on u over the range $0 > u > -1.3$ $(\mathrm{GeV}/c)^2$. The intermediate x point at positive u is definitely low; this is the most forward point represented, at $u - u_{\max} = 0.08$ $(\mathrm{GeV}/c)^2$. There is no other indication of u-dependent structure.

Figure 9(a) displays the data averaged over the interval $-0.05 > u > -0.90$ $(\mathrm{GeV}/c)^2$ as a function of x. Above $x = 0.55$ the asymmetry is constant but there is a marked decrease below this value. Indeed, the average value of the two points at x near 0.2 is negative.

The deuterium-target data are shown in Fig. 8(b), averaged over x as before. The asymmetry at small x is small and featureless. At the two larger x ranges, however, the asymmetry rises with increasing $|u|$, over the entire range at high x, and until $u = -0.8$ $(\mathrm{GeV}/c)^2$ at intermediate x.

D. K^- production

The data on the production of negative kaons are sparse, but at least one feature is illustrated in Fig. 9(b); an increase in the asymmetry as x increases. The data have been averaged over the interval $0.12 > u > -0.50$ $(\mathrm{GeV}/c)^2$. This increase is also noticeable in a plot of the asymmetry ver-

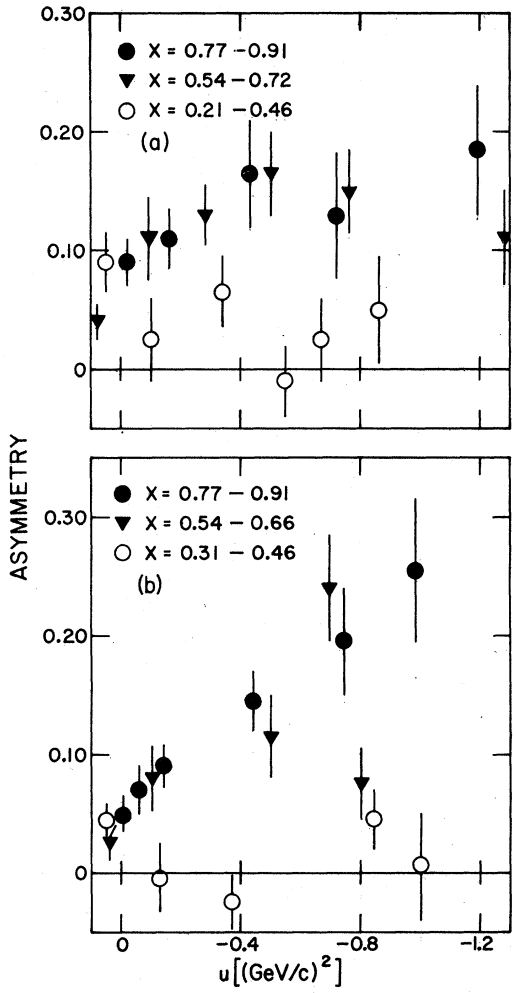

FIG. 8. The asymmetry for inclusive K^+ production from (a) hydrogen and (b) deuterium. Some of the data in Table III have been combined for these plots.

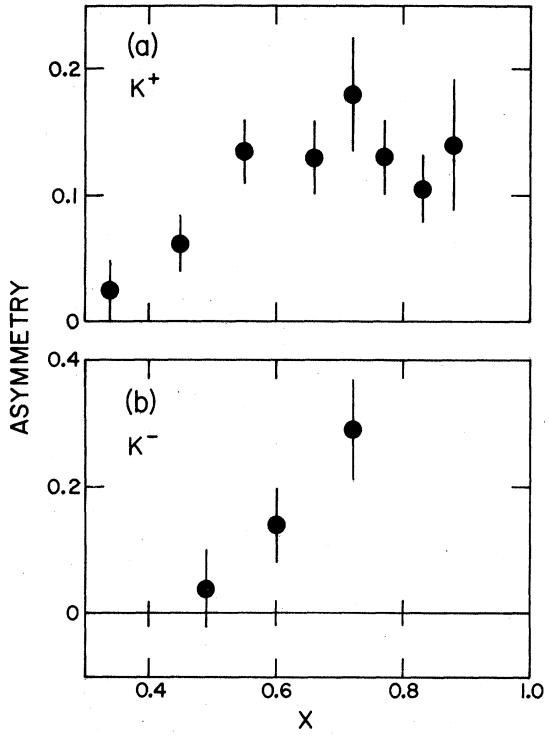

FIG. 9. (a) The asymmetry for inclusive K^+ production from hydrogen as a function of x. The data are the average asymmetry in the range $-0.05 > u > -0.90$ $(\mathrm{GeV}/c)^2$. (b) The inclusive K^- data averaged over the interval $0.12 > u > -0.50$ $(\mathrm{GeV}/c)^2$.

sus u in Fig. 10 where the data are combined into x ranges. There is no evident structure in u. The data from the deuterium-target runs are not shown; they are few but consistent with the hydrogen results.

E. Proton production

A portion of the hydrogen-target data listed in Table V is presented in Fig. 11(a) as a function of t. The elastic asymmetry data[9] show a dip in the region near $-t = 0.9$ $(\mathrm{GeV}/c)^2$ that is reflected in the inclusive data. The inclusive structure is much weaker, however, and weakest at the highest x value measured, 0.73. The two high x-data sets shown are, in fact, consistent with the assumption that the t dependence is flat.

The x dependence of the data is shown in Fig. 12(a) where the (interpolated) values of the asymmetry at two values of t are plotted as a function

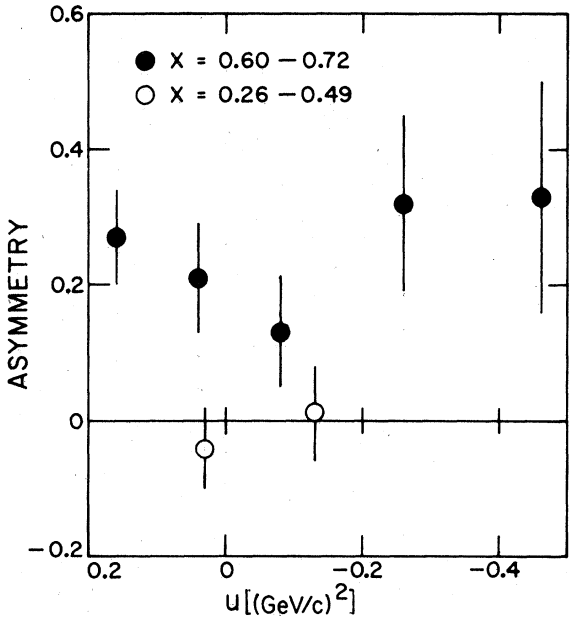

FIG. 10. The asymmetry for inclusive K^- production from hydrogen. The data are averaged over the indicated x intervals.

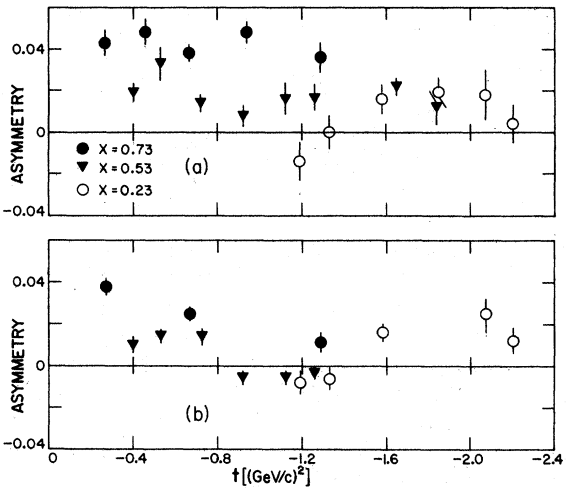

FIG. 11. The asymmetry for inclusive proton production from (a) hydrogen and (b) deuterium targets.

of x. The data at other t values are similar. There is an approximately linear increase in the asymmetry with x. If the extrapolation is carried to $x=1$, the value obtained is consistent with the average value[9] of the elastic asymmetry in the region covered by this data $(-0.2>t>-2.2)$ (GeV/c)^2.

A portion of the deuterium-target data is shown in Fig. 11(b). Again, there is an indication of structure in the data, with a possible dip in the region near $-t=1$ (GeV/c)^2. The data is, however, not consistent with the hydrogen results for $x>0.5$. In this region the deuterium asymmetries are substantially smaller than those from hydrogen, particularly at large t. This implies that the neutron-target asymmetry is (algebraically) smaller yet, which is also characteristic of elastic scattering.[10]

Figure 12(b) shows the interpolated values of the deuterium asymmetry for two values of t as a function of x. The asymmetry increases with increasing x, as before.

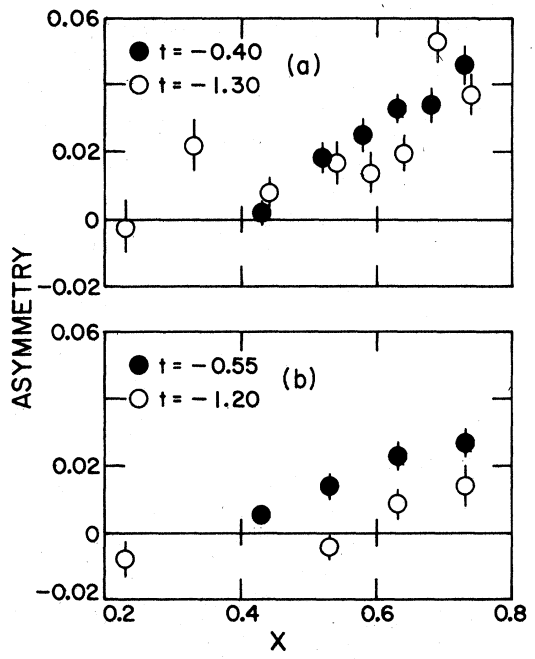

FIG. 12. The asymmetry for inclusive proton production at fixed t as a function of x from (a) hydrogen and (b) deuterium targets.

IV. DISCUSSION

In the absence of particularly relevant theoretical models, it is useful to summarize the phenomenological features of the data. These are

(a) The asymmetries for meson production are large and, when plotted as a function of u, show a consistent structure, whose major features are independent of x.

(b) The asymmetries are always small at small x and rise at large x.

(c) When compared with the data in Ref. 8, the asymmetries for meson production are similar at 6 and 11.75 GeV/c, when compared at the same values of x and u.

(d) The asymmetries for meson production are largely independent of the I_z of the target nucleon.

(e) The asymmetries for proton production are generally smaller than for elastic scattering, are dependent on the incident energy and the composition of the target, and show an approximately linear dependence on x.

We must now review the possible models for these processes to determine if any of their predictions are compatible with these features.

The naive picture of inclusive pion production in proton-nucleon collisions is that the incident proton strikes a virtual pion in the cloud surrounding the nucleon. An immediate consequence of this view is that while the probability of such a process is related to the properties of the target particle, the dynamics of the scattering should be comparable to the baryon-exchange process of backward elastic scattering of pions from protons, independent of the actual inclusive production target. In particular, the asymmetry for inclusive production of $\pi^\pm$ from proton-proton or proton-deuteron scattering should be similar to the asymmetry in backward $\pi^\pm p$ elastic scattering. The highest-momentum data for this process are those of Ref. 11 at 6 GeV/c, shown in Fig. 13. (The data have been consolidated and the necessary sign change in the translation from polarized-target to polarized-beam data has been included.)

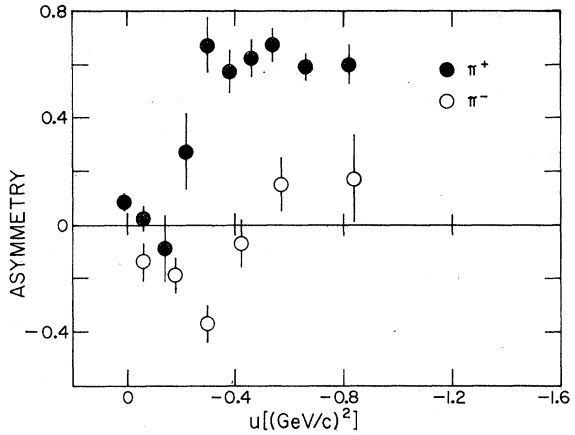

FIG. 13. The data of Ref. 11 for the asymmetry in backward $\pi^{\pm}$ proton elastic scattering (rebinned and with a sign change.)

The general similarities between the data sets are clear: small asymmetries near $u=0$, a large positive value at large $-u$ for π^+, and a more gradual rise in the asymmetry for π^-. The situation near $u=0$ is unclear [the maximum u for the elastic data is $+0.06$ $(\mathrm{GeV}/c)^2$ while the inelastic data begin at $+0.25$ $(\mathrm{GeV}/c)^2$ for π^+ and $+0.35$ $(\mathrm{GeV}/c)^2$ for π^-], but the points at which the asymmetry crosses zero are in substantial agreement. One major difference is in the rate that the π^+ asymmetry increases with $|u|$ and the value it achieves; for $u<-0.3$ $(\mathrm{GeV}/c)^2$ the elastic asymmetry is large (0.62) and constant, while the inelastic asymmetry (at $x=0.9$) does not achieve its somewhat lower maximum value until $u=-0.7$ $(\mathrm{GeV}/c)^2$.

The similarities that exist between the elastic and inclusive processes can be understood as a similarity between different processes dominated by baryon exchange.[12] Ader *et al.*[13] have shown that the asymmetry for a baryon-exchange process at high energy is simply expressed in terms of the total amplitude for exchange of a given naturality

$$A=\frac{-|N|^2+|U|^2}{|N|^2+|U|^2}\ ,$$

where N (U) is the amplitude of natural (unnatural) parity exchange. This implies that a single dominant amplitude leads to a unit asymmetry (in strong contrast to meson-exchange processes where an interference effect produces the asymmetry.) If the amplitudes are parametized in terms of natural and unnatural parity exchange u-dependent couplings $\beta_{N,U}(u)$ for the π-p vertex and $B_{N,U}(u,m_x^2)$ for the p-X inelastic vertex, the expressions for the asymmetry are

$$A_{\mathrm{el}}=\frac{|\beta_U(u)|^4-|\beta_N(u)|^4}{|\beta_U(u)|^4+|\beta_N(u)|^4}\ , \tag{1}$$

$$A_{\mathrm{inel}}=\frac{|\beta_U(u)B_U(u,m_x^2)|^2-|\beta_N(u)B_N(u,m_x^2)|^2}{|\beta_U(u)B_U(u,m_x^2)|^2+|\beta_N(u)B_N(u,m_x^2)|^2}\ . \tag{2}$$

These processes are diagrammed in Fig. 14(a) and 14(b). If the exchanged particle is denoted R, then the amplitude B describes R-p scattering, and when the sum over all final inelastic states is performed, B describes the total Rp cross section. It is reasonable to assume that natural and unnatural parity exchanged particles have roughly equivalent total cross sections, and thus that Eq. (2) simplifies so that

$$A_{\mathrm{inel}}\approx\frac{|\beta_U(u)|^2-|\beta_N(u)|^2}{|\beta_U(u)|^2+|\beta_N(u)|^2}\ . \tag{3}$$

This expression has zeros at the same value of u as does expression (1) for the elastic asymmetry as well as the same sign, although the magnitudes and the u dependence away from the zeros may be quite different. In addition, if the amplitude B' which represents inelastic R-neutron scattering has similar properties, the expression for the inelastic asymmetry from a neutron target will also be expression (3), and the asymmetries from deuterium should resemble those from hydrogen. These features are, of course, present in our data.

It should be emphasized that the discussion

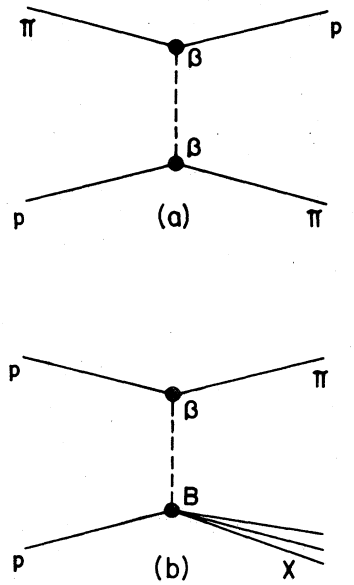

FIG. 14. (a) A baryon-exchange diagram for backward πp scattering. (b) For inclusive pion production.

above is based on the expectation that the general structure of the backward elastic pion asymmetry data (especially the signs and locations of zeros) are not strong functions of energy in the region of comparison (6 to 12 GeV). As noted above, it appears that the inclusive pion asymmetries are similar at these two energies.

One feature of the data that is not addressed by this model is the strong (and variable) x dependence. Of course, Fig. 14 exhibits only the lowest-order diagrams of any real theory; cut contributions could very easily be important and strongly x dependent. Alternatively, π-meson production at low x is most certainly dominated by the process $pp \to pN^* \to p\pi X'$, where X' represents the other decay products of the resonance N^*. The x dependence is then explained as a dilution effect, assuming that the pions produced by the reaction are largely isotropic.

The arguments presented above apply equally well to the cases of kaon production from hydrogen and deuterium. Unfortunately, there is no backward elastic asymmetry data for the kaon-proton system at momenta above 3 GeV/c. We predict that the asymmetry for both K^+ and K^- proton scattering should be positive and featureless. There is some indication of a qualitative difference between the K^+ production data from hydrogen and deuterium [see Fig. 8(a) and 8(b)], but the data are inconclusive.

For the case of proton production, a theory for the inclusive asymmetry has been proposed based on the triple-Regge formulation[3]

$$A\,\frac{d^2\sigma}{dt\,dm_X^{\,2}} = \frac{1}{s^2}\sum_{ijk}\tilde{P}_{ijk}(t)\left(\frac{s}{\nu}\right)^{\alpha_i(t)+\alpha_j(t)}\nu^{\alpha_k(0)}, \tag{4}$$

which corresponds to the diagram of Fig. 15. The residue function $\tilde{P}_{ijk}$ vanishes if the Regge poles i and j are equal, have the same phase or differing naturalities. The variables are s, the square of the total center-of-mass energy, t, the square of the four-momentum transfer, and $\nu = 2m_p(E_0 - E)$, the energy transfer. The expression is valid only if $m_X^2/s \ll 1$, and both m_X^2 and s are large, so that a strict test with our data is not possible. A previous experiment at 6 GeV/c (Ref. 4) has investigated the inclusive asymmetry in proton production by calculating finite-mass-sum-rule (FMSR) integrals to partially offset the disadvantages of small m_X^2 (3 GeV^2) and s (13.2 GeV^2). The present data are at considerably larger values of these variables, m_X^2 near 7.5 GeV^2 and $s = 24$ GeV^2, but the ratio is near 0.3, not extremely small.

The dominant trajectories are expected to be

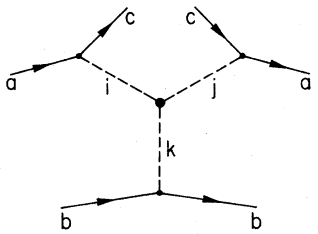

FIG. 15. The Mueller-Regge diagram for inclusive production $ab \to cX$. Regge trajectories i, j, and k are identified in the text for the case in which a, b, and c are protons.

$ijk = P\rho\rho$ and PA_2A_2 where P represents the Pomeron. It is also possible that $f\rho\rho$ and fA_2A_2 are important as well. If these latter are neglected, Eq. (4) predicts that

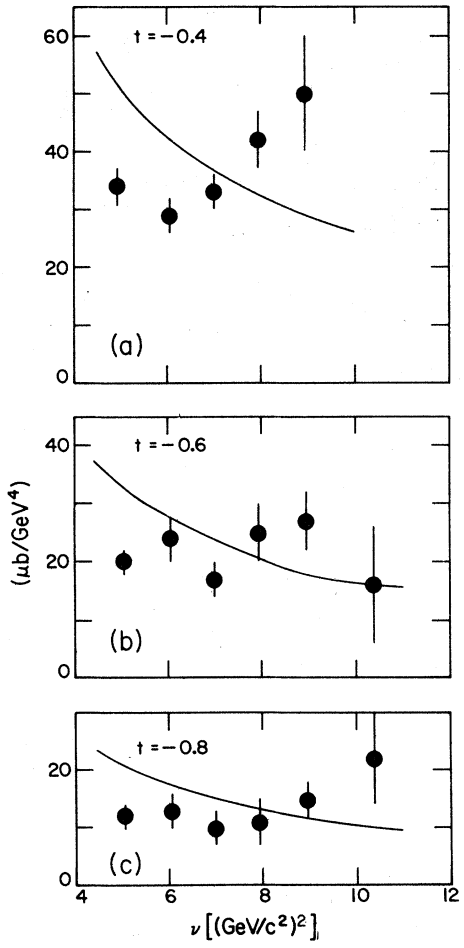

FIG. 16. The product of the cross section $d^2\sigma/dt\,dm_X^2$ and the asymmetry for inclusive proton production from hydrogen at fixed momentum transfer. The naive triple-Regge prediction, $A\sigma \propto 1/\nu$, normalized to the experimental data, is also indicated. The cross-section data have been taken from Ref. 1.

$$A \frac{d^2\sigma}{dt\, dm_X^2} \propto \frac{1}{\nu} \tag{5}$$

at fixed s and t. This quantity is presented in Fig. 16(a)–16(c), for three values of t. Since our data do not include low-m_X^2 points, the FMSR integrals cannot be evaluated. The cross-section data, taken from Ref. 1, rise as a function of ν and the asymmetry values fall, but insufficiently quickly in order to force the product to fall. A $1/\nu$ dependence, adjusted to fit the average value is shown superimposed on the data. The best agreement is at large t, but the χ^2 values are not impressive. A further complication develops at high ν: the asymmetry becomes negative for $\nu > 12$ GeV^2. There is no way to accomodate this behavior in the simple version of the theory outlined above.

ACKNOWLEDGMENTS

We are grateful to the Argonne ZGS staff for the successful operation of the polarized beam. We thank A.B. Wicklund, G. Thomas and D. Geffen for helpful conversations and J. Lee, E. Marquit, W. Petersen, T. Walsh, and E. Haqq for their help with the experiment. Thanks are also due to L. E. Price and J. Broadhurst for providing equipment and assistance, and G. Phillips for his encouragement and support. This work was supported by the U. S. Energy Research and Development Administration and by the Graduate School of the University of Minnesota.

[1] C. W. Akerlof *et al.*, Phys. Rev. D 3, 645 (1971) and references contained therein.
[2] D. G. Crabb, in *High Energy Physics with Polarized Beams and Targets*, proceedings of the Argonne Symposium, 1976, edited by M. L. Marshak (AIP, New York, 1976), p. 104.
[3] R. D. Field, in Proceedings of the Summer Study on High Energy Physics with Polarized Beams [Argonne National Laboratory Report No. ANL/HEP 75-02, 1975 (unpublished)]. See also, F. E. Paige and D. P. Sidhu, Phys. Rev. D 14, 2307 (1976).
[4] D. S. Ayres *et al.*, Phys. Rev. D 15, 1826 (1977).
[5] This polarimeter is described by K. Abe, Ref. 2, p. 114.
[6] The left and right arms of the polarimeter were almost exactly symmetric, which ensures that this form is an accurate representation of the beam polarization. A more complicated representation is discussed in Ref. 4.
[7] R. D. Klem *et al.*, Phys. Rev. D 15, 602 (1977).
[8] R. D. Klem *et al.*, Phys. Rev. Lett. 36, 929 (1976) and the article by J. B. Roberts in Ref. 2, p. 219.
[9] See, for example, Ref. 5.
[10] A. B. Wicklund, private communication.
[11] L. Dick *et al.*, Nucl. Phys. B43, 522 (1972); B64, 45 (1973).
[12] This treatment of baryon exchange was suggested by A. B. Wicklund.
[13] J. P. Ader, C. Meyers, and Ph. Salin, Nucl. Phys. B58, 621 (1973).